ACTA CHEMICA IASI, **34_1**, 110-147 (2026)
DOI: 10.47743/achi-2026-1-0005

Article

SELF-ASSEMBLED CHITOSAN-PEG NANOCARRIERS FOR *CORDYCEPS MILITARIS* EXTRACT: PROCESS OPTIMIZATION AND ENHANCED BIOLOGICAL ACTIVITIES

Quoc-Thang Nguyen and Quang-Hieu Tran*

Faculty of Chemical Engineering, Industrial University of Hochiminh City, 12 Nguyen Van Bao, Hanh Thong Ward, Hochiminh City 700000, Vietnam

Abstract: *Cordyceps militaris* (*C. militaris)* is renowned for its valuable bioactive compounds, notably Cordycepin (COR) and Adenosine (ADE). However, these compounds suffer from poor stability and low bioavailability, which limit their therapeutic potential. This study successfully developed a self-assembled nano-delivery system based on a Chitosan-polyethylene glycol (PEG) matrix to encapsulate *C. militaris* extract. The formulation was optimized by evaluating the effects of the Chitosan/PEG mass ratio, surfactant concentration (Tween 80), and processing parameters including stirring speed and phase inversion temperature. The optimized nanoparticles achieved an ultra-small average particle size of 14 ± 3.7 nm with a polydispersity index (PDI) of 0.31. High-performance liquid chromatography (HPLC) analysis confirmed high encapsulation efficiencies of 72.4 % for COR and 65.2 % for ADE. Transmission Electron Microscopy (TEM) revealed that the nanoparticles possessed a spherical morphology and a uniform distribution. Stability studies indicated that the nano-system maintained its

* Quang-Hieu Tran, *e-mail:* tranquanghieu@iuh.edu.vn

physical integrity for over 30 days. Furthermore, the encapsulated extract demonstrated significantly enhanced antibacterial activity against *Staphylococcus* aureus and *Escherichia coli*, as well as superior antioxidant capacity compared to the crude extract. These results suggest that the Chitosan-PEG nano-platform is a highly effective vehicle for improving the stability and biological performance of *C. militaris* bioactives in pharmaceutical and functional food applications.

Graphical abstract

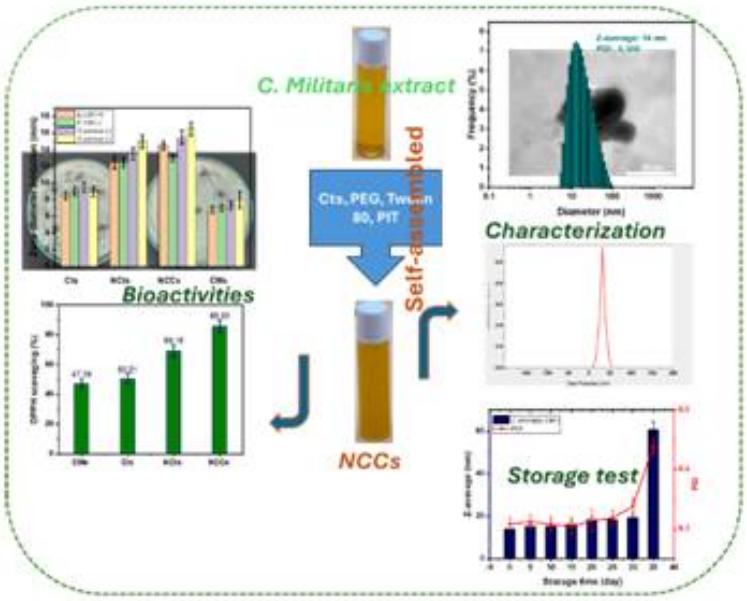

Keywords: *Cordyceps militaris*, nano-system, Adenosine, Cordycepin, Chitosan, PEG, Tween 80, antioxidant activity, antibacterial activity.

Introduction

Cordyceps militaris, a prized medicinal mushroom, has been extensively utilized in traditional Asian medicine for thousands of years.[1] With its diverse biological activities, including anti-inflammatory, anti-tumor, antioxidant, immunomodulatory, and organ-protective properties, *Cordyceps militaris* has garnered significant attention from the modern scientific community.[2] Research indicates that this fungus contains a

substantial amount of valuable bioactive compounds, notably Adenosine (ADE) and Cordycepin (COR). ADE plays a crucial role in various physiological processes related to cellular energy and neural signaling, with potential benefits for sleep quality improvement and cardiovascular function.[3] COR, a 3'-deoxyadenosine derivative, is a characteristic bioactive compound of *Cordyceps* that exhibits potent pharmacological properties such as antibacterial, anti-cancer, and immunoregulatory effects.[4]

Despite their high pharmacological potential, ADE and COR face significant challenges regarding their bioavailability upon administration. They are highly susceptible to enzymatic degradation within the body, for instance, by Adenosine Deaminase (ADA), and are rapidly eliminated, especially via oral routes.[5,6] The harsh acidic environment of the stomach and oxidative stress factors further contribute to the reduced efficacy of these active compounds before they can exert their effects on target tissues.[7] This underscores the critical need for developing efficient delivery and protective systems to enhance their bioavailability and prolong their therapeutic action.

Nanotechnology has emerged as a promising solution to address these challenges. Nano-delivery systems, with their ultra-small size (typically 1 - 100 nm), are capable of encapsulating active compounds, protecting them from degradation, enhancing absorption across biological membranes, and enabling controlled release.[8,9] Among various nanomaterials, polymeric nanoparticles are particularly attractive due to their versatility, biocompatibility, and low toxicity. Chitosan (Cts), a natural polysaccharide derived from shrimp and crab shells, is an ideal biomaterial owing to its biocompatibility, biodegradability, non-toxicity, and inherent antibacterial properties.[10] The polycationic nature of Cts facilitates its interaction with negatively charged cell membranes, thereby promoting drug transport across biological barriers.[11] Polyethylene glycol (PEG) is

commonly used to stabilize nanoparticles by forming a steric barrier around the particles, preventing aggregation.[12] Tween 80, a non-ionic surfactant, plays a vital role in reducing interfacial tension and forming small, uniform nanoparticles.[13]

Although nano-encapsulated *Cordyceps militaris* extracts have recently gained increasing attention utilizing various polymer matrices, [11,14,15] studies focusing on their encapsulation via low-energy self-assembly methods for food-grade delivery remain notably limited. In previous works, our group developed double emulsion nano-systems and liposomal nano-systems to load these active compounds, demonstrating significantly improved biological properties in both *in vitro* digestion and *in vivo* studies.[16,17] In this current study, we propose a novel nano-system based on non-ionic surfactants to co-encapsulate chitosan and *Cordyceps militaris* extract, aiming to diversify material options for developing application-oriented products in pharmaceuticals and dietary supplements. Based on the aforementioned rationale, this research was conducted with the primary objectives of developing and optimizing a complex nano-system containing *Cordyceps militaris* extract using a combination of Cts, PEG, and Tween 80, by systematically investigating factors influencing nanoparticle size and polydispersity. Furthermore, the study aimed to characterize the morphology and structure, assess the physical stability, and evaluate the antioxidant and antibacterial activities of the optimized *C. militaris* nano-system to demonstrate its potential applications. The findings of this study are expected to provide an effective approach to enhance the bioavailability and bioactivity of active compounds from *Cordyceps militaris*, thereby expanding its potential applications in health-protective functional foods and pharmaceutical products.

1. Materials and methods

1.1. Raw materials and chemicals

C. militaris powder was generously supplied by Thien An company (Dong Thap province, Vietnam), cultivated on a substrate of brown rice and pupae. Chitosan (Cts) (low molecular weight, ~150 kDa; degree of deacetylation (DD) ≥ 85 %) was purchased from Biobasic (Canada). PEG - 400 (Polyethylene glycol) and Tween 80 (Polysorbate 80), a non-ionic surfactant employed as an emulsifier and system stabilizer, were acquired from Sigma Aldrich (USA). Analytical standards of Adenosine ($C_{10}H_{13}N_5O_4$, purity > 96 %) and Cordycepin ($C_{10}H_{13}N_5O_4$, 98 %) were obtained from Sigma Aldrich (USA). Ethanol 96°, glacial acetic acid, and other analytical-grade chemicals, such as DPPH and HPLC solvents, were sourced from similar reputable suppliers and met analytical standards.

1.2. Preparation of chemical solutions

The preparation of chemical solutions involved two key steps. Firstly, a 0.35 % (w/v) Cts solution was prepared by completely dissolving 0.35 g of chitosan in 100 mL of 1 % (v/v) acetic acid solution. This mixture was then continuously stirred for 24 hours until a homogeneous solution was achieved. Secondly, a 0.5 % (w/v) PEG solution was made by dissolving 0.5 g of PEG - 400 in 100 mL of hot distilled water (maintained at approximately 60 - 70 °C) and stirring until the PEG was completely dissolved.

1.3. Extraction of ADE and COR

The extraction protocol for ADE and COR was meticulously performed following our previously established and published methodology.[18] In brief, 1.0 g of *C. militaris* powder was precisely weighed and then dispersed in 20 mL of water. The mixture was subsequently vortexed for 2 min to ensure uniform dispersion, followed by sonication at a power of 450W for 60 seconds. Following this, the sample was placed in a thermostatic bath and subjected to extraction at 60 °C for 90 min. After the

extraction phase, the mixture underwent centrifugation at 3500 rpm for 10 min to effectively remove insoluble residues. The resulting supernatant extract was filtered, and the entire extraction procedure was meticulously repeated 2-3 times with the remaining solid residue to guarantee exhaustive extraction of the target active compounds.

1.4. Preparation of *C. militaris* nano-system (NCCs) via self-assembly

The NCCs were fabricated using a self-assembly mechanism facilitated by an emulsification-diffusion process under precise thermal and mechanical control. Initially, a polymer matrix was established by blending 28 g of 0.35 % (w/v) Cts and 12 g of 0.5 % (w/v) PEG - 400 to achieve a Cts:PEG weight ratio of 7:3. Into this matrix, 3.0 g of concentrated *C. militaris* extract (vacuum-concentrated to 25 °Brix) was thoroughly incorporated. This bioactive aliquot, derived from a 1:20 (w/v) aqueous extract, provided a standardized input of 9.0 mg ADE and 11.25 mg COR (m_0) to serve as the baseline for subsequent encapsulation efficiency assessments. The resulting mixture was then heated to 70 °C and continuously stirred at 900 rpm for 30 min. This critical activation stage facilitated the uncoiling and stretching of polymer chains, promoting the formation of non-covalent hydrophobic interactions and hydrogen bonding with the bioactive nucleosides, which effectively initiated the hierarchical self-assembly process.

Subsequently, 2.0 g of Tween 80 was incorporated into the system to reduce interfacial tension and provide steric stabilization for the nascent nanostructures during an additional 30 min of stirring. To effectively "lock" the bioactive compounds within the polymeric framework, the mixture was subjected to a rapid "thermal shock" by cooling to 15 °C, which decreased localized solubility and solidified the nano-frame. The final homogenization was achieved through probe ultrasonication at 450 W (VCX-750) for 2 min in an ice bath. This crucial step ensured the complete dispersion of any potential aggregates, ultimately yielding a highly homogeneous nano-

suspension with target particle sizes significantly below 200 nm, consistent with the requirements for advanced ultrasound-assisted nano-formulations.

1.5. Optimization of NCCs formulation and processing parameters

The preparation of NCCs was optimized using a sequential single-factor design to evaluate the impact of various parameters on the mean particle size (Z-average) and polydispersity index (PDI). Five key factors were investigated: Cts:PEG weight ratio, Tween 80 concentration, preparation temperature, stirring speed, and stirring time. In this approach, the optimal level identified for each factor was utilized as a fixed constant for the subsequent optimization stages. The detailed experimental matrix, including investigated ranges and constant operating conditions, is summarized in Table 1.

Table 1. Experimental design for the sequential single-factor optimization of NCCs processing parameters.

Step	Investigated factor	Variable levels	Constant operating parameters
1	Cts:PEG weight ratio	5:5, 7:3, 9:1	Extract: 3.0 g; Tween 80: 2.0 g; Temp: 70 °C; Speed: 900 rpm; Time: 30 min
2	Tween 80 concentration	1, 2, 3, 4, 5, 6, 7 % (w/v)	Extract: 3.0 g; **Cts:PEG ratio***; Temp: 70 °C; Speed: 900 rpm; Time: 30 min
3	Preparation temperature	60, 65, 70, 75, 80 °C	Extract: 3.0 g; Cts:PEG ratio*; **Tween 80***; Speed: 900 rpm; Time: 30 min
4	Stirring speed	600, 750, 900, 1050, 1200 rpm	Extract: 3.0 g; Cts:PEG ratio*; Tween 80*; **Temp***; Time: 30 min
5	Stirring time	20, 25, 30, 35, 40 min	Extract: 3.0 g; Cts:PEG ratio*; Tween 80*; Temp*; **Speed***

Note: *Factors marked with an asterisk (*) were fixed at the optimal levels determined from the immediately preceding step. All formulations underwent standardized downstream processing: thermal shock (15 °C) and probe ultrasonication (450W, 2 min, ice bath). Target responses include Z-average size (nm) and Polydispersity Index (PDI).*

1.6. Quantification of ADE and COR by HPLC-DAD

The accurate quantification of ADE and COR content was achieved through high-performance liquid chromatography coupled with diode array detection (HPLC - DAD), specifically using an Agilent 1260 Infinity II system. The analytical conditions were precisely set as follows: a ODS - C18 column (250 mm x 4.6 mm, 5 µm) was employed, with the column temperature maintained at 30°C. The mobile phase consisted of a carefully prepared mixture of acetonitrile and phosphate buffer pH 6.5, in a ratio of 8:92 (v/v). A constant flow rate of 0.6 mL/min was maintained, and the injection volume for each sample was 20 µL. Detection of the compounds was performed at a wavelength of 260 nm. Standard calibration curves were meticulously constructed by serially diluting standard ADE and COR solutions at various known concentrations and subsequently measuring their corresponding peak areas.

1.7. Determination of encapsulation efficiency (EE %)

The encapsulation efficiency (EE %) was determined using an indirect method, which involved the separation of free, unencapsulated active compounds from the nanoparticles which was referred from previous works.[9,19] A 2.0 mL sample of the NCCs was transferred into a centrifuge tube fitted with an ultrafiltration membrane, characterized by a molecular weight cut-off (MWCO) of 10.0 kDa. This sample was then subjected to centrifugation at 5000 rpm for a duration of 10 min. The resulting filtrate, which contained the free active compounds, was carefully collected, and its ADE and COR content was quantified using the HPLC-DAD method described previously. The encapsulation efficiency was subsequently calculated using the following formula:

$$EE\ \% = [(A_{total} - A_{free}) / A_{total}] \cdot 100$$

where A_{total} represents the total amount of ADE or COR initially present in the crude extract, and A_{free} denotes the amount of ADE or COR that was not encapsulated and remained free in the filtrate.

1.8. Characterization of nano-system physical properties

The physical attributes of the nano-system, specifically the mean particle size (Z-average) and polydispersity index (PDI), were accurately determined through dynamic light scattering (DLS) utilizing a HORIBA SZ-100 instrument (Japan). Prior to measurement, samples were carefully diluted with deionized water to prevent any interference from excessive light scattering effects. The Zeta potential, a crucial indicator of surface charge and colloidal stability, was measured using the same DLS instrument. The morphology and internal structure of the nanoparticles were meticulously observed using transmission electron microscopy (TEM), specifically with a JEM-1010 instrument (JEOL, Japan), at the Central Institute of Hygiene and Epidemiology, Vietnam. For TEM sample preparation, a minute drop of the nano-solution was carefully placed onto a carbon-coated copper grid and then allowed to air-dry at room temperature before observation.

1.9. Evaluation of storage stability

The storage stability of the Chitosan-PEG nano-system loaded with *C. militaris* extract was comprehensively investigated to ascertain its capacity to maintain particle structure and the integrity of its active compound content under defined storage conditions. Nano-suspension samples were meticulously stored in sealed glass vials under 4 °C and ambient temperature (25 °C), for an extended period of 30 days. Periodically, at 5-day intervals, critical parameters including mean particle size (Z-average), polydispersity index (PDI), were re-analyzed using the DLS method. Concurrently, any observable macroscopic changes such as phase separation, discoloration, or precipitation were visually recorded.

1.10. Evaluation of biological activity

1.10.1. Antibacterial activity

The antibacterial activity was rigorously evaluated using the standard agar disc diffusion method against two representative bacterial strains: *Escherichia coli* (a Gram-negative bacterium) and *Staphylococcus aureus* (a Gram-positive bacterium).[20] The tested samples included the *C. militaris* extract, neat chitosan, nano-chitosan, and the optimized NCCs nano-system. To ensure a scientifically rigorous comparison, the concentrations of the control samples (crude extract and nano-chitosan) were adjusted to be strictly equivalent to the respective amounts embedded within the 0.4 % (w/v) NCC formulation, rather than employing a generic uniform weight percentage. Bacterial cultures were spread evenly on Mueller-Hinton agar plates. Paper discs impregnated with 10 µL of each sample solution were carefully placed onto the agar surface. The plates were then incubated at 37 °C for 24 hours, after which the diameter of the inhibition zone (measured in millimeters) around each disc was recorded.

1.10.2. Antioxidant activity (DPPH)

The antioxidant activity of the *C. militaris* extract, NCCs and individual composition for developed nano-system was assessed by their capacity to scavenge DPPH free radicals at 0.4 % (w/v) as previous works.[21 – 23] This evaluation was conducted following our previously published protocol, with absorbance measurements taken at 517 nm. The percentage of DPPH radical inhibition was subsequently calculated to quantify the antioxidant efficacy.

2. Results and discussion

2.1. Investigation of factors affecting nano-system size

In the realm of pharmaceutical nano-technology, particle size and polydispersity index (PDI) are two unequivocally critical parameters that fundamentally dictate the long-term stability of nano-suspensions, influence drug release profiles, and significantly impact targeting efficiency. An ideal nano-system is typically characterized by a small particle size, generally below 200 nm, coupled with a low PDI, ideally less than 0.3, to ensure both homogeneity and optimal stability, as highlighted in literature concerning crucial parameters in polymeric nanocarriers.[24]

2.1.1. Effect of Cts and PEG ratio

To systematically establish the structural foundation of the self-assembled nutraceutical delivery platform, the influence of the Chitosan to PEG-400 weight ratio was comprehensively evaluated while keeping all processing and interfacial parameters constant, as systematically cross-referenced in Table 2. The resulting hydrodynamic size distribution profiles for the three designated matrix formulations (5:5, 7:3, and 9:1) are comparatively visualized on a logarithmic scale in Figure 1A. The experimental data revealed a non-linear, threshold-driven relationship, demonstrating that the structural evolution of the nanocarriers is strictly governed by the macromolecular stoichiometry between the biopolymer backbone and the plasticizing polyol matrix.

As illustrated in Figure 1A, the formulation prepared at a balanced Cts:PEG weight ratio of 5:5 yielded a broad, heavily diffused distribution profile with a primary peak mean positioned at 20.1 ±14.1 nm but displaying a heavily distorted, sub-micron cumulative Z-average of 927.9 nm (PDI = 0.547). This prominent structural discrepancy represents a textbook intensity-weighted artifact typical of dynamic light scattering (DLS) operations. At this specific compositional equilibrium, an excessive concentration of PEG-400 molecules promotes inter-chain bridging across

adjacent Chitosan backbones. This phenomenon initiates the formation of a minor population of loose, highly extended, and heavily hydrated macromolecular aggregates. Because the light scattering intensity mathematically scales with the sixth power of the particle hydrodynamic diameter ($I \propto d^6$), these larger localized aggregates heavily dominate the light scattering signals, dragging the cumulative Z-average into the sub-micron domain while the primary population of uncomplexed polymeric segments remains clustered at a lower boundary.

A sudden and remarkable structural contraction was captured when the formulation matrix shifted to the optimal Cts:PEG weight ratio of 7:3. As plotted in Figure 2A, the hydrodynamic distribution condensed into an exceptionally sharp, uniform, and highly symmetric Gaussian curve, exhibiting a localized Z-average of 14.1nm and a peak mean diameter of 20.1±14.1 nm with a significantly narrowed polydispersity index (PDI = 0.366). At this critical thermodynamic sweet spot, the spatial stoichiometry between the highly protonated amine segments (-NH_3^+) of the food-grade Chitosan (DD ≥ 85 %) and the polar ether domains of PEG-400 reaches a perfect charge-to-volume balance. The removal of excessive polyol bridging triggers immediate, spontaneous intramolecular chain-folding.[25] This spatial collapse drives the biopolymer network into tightly packed, condensed core-shell micellar configurations, which are simultaneously locked and thermodynamically stabilized by the interfacial steric barrier provided by Tween 80 at the designated Phase Inversion Temperature (PIT).

Conversely, further restricting the plasticizing spacer by moving to a Cts:PEG weight ratio of 9:1 caused the hydrodynamic dimensions to bounce back upward, expanding the distribution profile to a peak mean diameter of 271.2 ±133.2 nm and a cumulative Z-average of 384.1 nm, (PDI = 0.449). This structural expansion is driven by a severe deficiency of PEG-400 molecules to act as steric fluidizers and intermolecular shielding agents. [26] Left unshielded, the immense density of positive charges along the

dominant Chitosan backbone generates powerful intra-molecular electrostatic repulsions. These repulsive forces forbid the polymer chains from executing the necessary folding configurations, forcing the macromolecular framework into a rigid, extended conformation that swells within the aqueous medium.

Taken together, the characteristic "V-shaped" dimensional trajectory explicitly validated that the structural framework outlined in Table 2 successfully localized the Cts:PEG 7:3 ratio as the absolute energetic and thermodynamic boundary required to engineer ultra-small, stable nano-food delivery architectures.

Table 2. Influence of Cts:PEG weight ratio on the mean particle size (Z-average) and polydispersity index (PDI) of the NCCs.

Cts:PEG (w/w)	Peak 1 Mean (nm)	Z-average Mean ± SD (nm)	PDI Mean ± SD
5:5	149.5 ± 98.8 [a]	927.9 ± 98.8[a]	0.547 ± 0.021[a]
7:3	20.1 ± 14.1 [c]	14.1 ± 14.1[c]	0.366 ± 0.015[c]
9:1	271.2 ± 133.2 [b]	384.1 ± 133.2[b]	0.449 ± 0.018[b]

Note: Data are expressed as Mean ± Standard Deviation (SD). Superscript letters (a, b, c) within the same column indicate statistically significant differences ($p < 0.05$) determined by Analysis of Variance (ANOVA) followed by Tukey's post-hoc test.

2.1.2. Effect of Tween 80 concentration

The concentration of the surfactant, Tween 80, was identified as a pivotal factor in meticulously controlling particle size.[13,27] Its function is two-fold: reducing interfacial tension between phases and establishing a robust barrier that effectively impedes the coalescence of polymer nano-droplets. The detailed results delineating the variation in particle size with increasing Tween 80 concentration (ranging from 1 % to 7 % w/v) are comprehensively presented in Figure 1B. As depicted in Figure 1B, a discernible decreasing trend in nano-particle size was observed with escalating Tween 80 concentrations (see more detail in Figure S4, S5, S6 and S7). At a low concentration of 1 %, the mean particle size remained

relatively large at 61.3 nm. More critically, the DLS profile for this concentration exhibited a secondary peak at 67.9 nm, strongly indicating an unstable and heterogeneous dispersion. This phenomenon is attributable to an insufficient amount of Tween 80 at lower concentrations to fully cover the surface of the polymer/extract droplets.

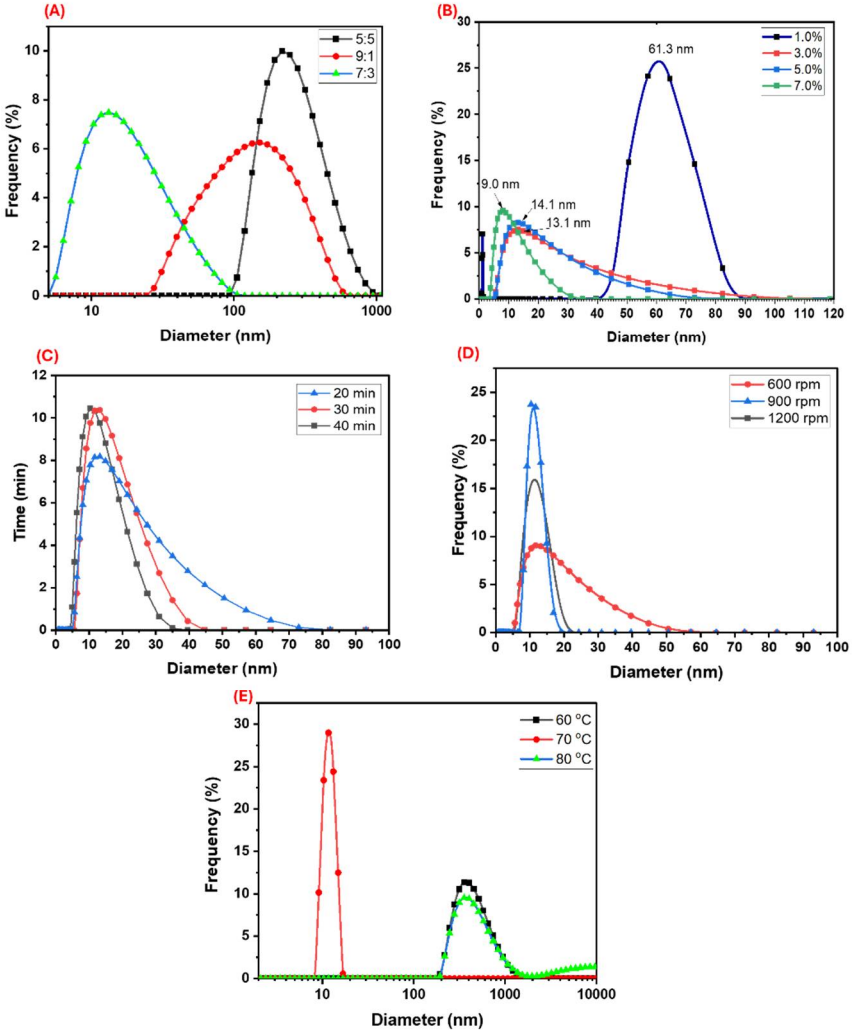

Figure 1. Systemic optimization of formulation and processing parameters tracking the hydrodynamic dimensions of the self-assembled nanocarriers (NCCs): (A) Chitosan to PEG-400 weight ratio (5:5, 7:3, and 9:1 plotted on a logarithmic scale), (B) Tween 80 surfactant concentration, (C) mechanical stirring time, (D) mechanical stirring speed, and (E) phase inversion temperature (PIT). Profiles represent intensity-weighted particle size distributions derived from dynamic light scattering (DLS) analysis.

This leads to high interfacial tension, which, in turn, promotes the coalescence of individual particles into larger aggregates. Conversely, upon increasing the Tween 80 concentration to 3 %, the particle size dramatically decreased to an optimal 14.1 nm, accompanied by a low PDI of 0.366, which robustly signifies a highly homogeneous and stable system. With an ideal Hydrophilic-Lipophilic Balance (HLB) typically ranging between 15 and 18, Tween 80 functions as an exceptionally effective non-ionic surfactant. Its role is not merely confined to reducing surface energy but critically extends to forming a saturated steric protective layer around the Chitosan-PEG core.[28,29]

This capability for superior dispersion is particularly evident when contrasted with traditional ionotropic gelation methods, such as those employing Chitosan-TPP, which typically yield particles in the larger range of 150 to 278 nm as reported by Karimi et al. (2013).[30] Our self-assembled system, therefore, demonstrates a distinct advantage, primarily due to the crucial support provided by Tween 80. At higher Tween 80 concentrations, specifically at 5 % and 7 %, the particle size continued to marginally decrease, reaching a minimum of 9.0 nm at 7 %. However, this incremental reduction was not statistically significant when compared to the results obtained at 3 %. Nevertheless, it is important to note that the overuse of surfactants beyond its critical micelle concentration (CMC) can lead to the formation of empty micelles. Such a scenario not only represents wastage of raw materials but also carries inherent risks of cytotoxicity or a reduction in active compound encapsulation efficiency due to spatial competition, as prudently cautioned by Tsujino et al. (1999).[31]

The refined process developed in this study not only successfully yields ultra-small particles, thereby enhancing biological permeation, but

also adheres to the fundamental principles of Green Chemistry. Unlike many nano-systems that frequently necessitate the use of complex organic solvents, the incorporation of Tween 80 within an aqueous environment effectively ensures both system stability and homogeneity. Consequently, after carefully considering technical efficiency, economic viability, and biological safety, a 3 % Tween 80 concentration was definitively identified as the optimal parameter for the preparation of the NCCs.

2.1.3. Effect of stirring time on NCCs formation

Mechanical interaction time during the emulsification process was found to significantly determine the equilibrium between the breakdown of polymer aggregates and the subsequent surface coverage of nascent particles. [32,33] The results presented in Figure 1C, S8, S9 and S10, which details particle size distribution at various stirring durations, clearly depict a typical bell-shaped curve, a common characteristic in nano-formulation processes. At a stirring time of 20 min, the particles exhibited a size of 100.9 nm with a high PDI of 0.540. This can be attributed to an insufficient energy input to overcome the intermolecular forces within the chitosan structure, thus preventing the complete uncoiling of polymer chains necessary for efficient active compound encapsulation.

Upon extending the stirring time to 30 min, a dramatic reduction in particle size to an optimal 12.2 nm was observed, with the PDI simultaneously reaching its lowest value of 0.308. This duration represents the "sweet spot" where adequate shear force is applied, effectively creating ultra-small nano-droplets. Concurrently, PEG and Tween 80 molecules are afforded sufficient time to arrange themselves, forming a robust protective layer that immediately prevents re-aggregation. However, prolonging the stirring time to 40 min resulted in an undesirable sharp increase in PDI to

0.500. This phenomenon reflects the system's inherent instability, likely due to excessive collisions between nanoparticles, a process intensified by increased Brownian motion, leading to coalescence or localized heat generation. Such heat can alter the conformation of the PEG shell, a finding consistent with the warnings issued by Trofa et al. regarding the energy limits in self-assembled systems.[34]

2.1.4. Effect of stirring speed

The stirring speed in the nano-formulation process serves as the primary source of mechanical shear force, which is essential for the effective deformation and breakup of polymer droplets into the nanometric range [35]. The results, as meticulously detailed in Figure 1D, S11, 12, and S13, provide an unequivocal demonstration of a critical energy density threshold required for optimal droplet disruption. At a stirring speed of 600 rpm, the observed particle size was 222.2 nm, indicating that the applied Laplace pressure was insufficient to overcome the interfacial tension and viscous forces inherent in the system.[36]

In contrast, increasing the stirring speed to 900 rpm induced a significant reduction in particle size to 12.4 nm. This observation suggests that 900 rpm provides sufficient shear stress to rapidly expand the interfacial surface area, allowing the surfactant molecules (Tween 80) to promptly adsorb onto and stabilize the newly formed interfaces, thereby preventing immediate recoalescence.[37,38]

Notably, a further increase in stirring speed to 1200 rpm resulted in an undesirable sharp increase in the PDI to 0.743, signifying a highly heterogeneous system. This destabilization is attributed to the phenomenon of acoustic or hydrodynamic cavitation and an intensified collision frequency between nascent nanoparticles. Excessive energy input at higher speeds generates turbulent flow conditions that can disrupt the protective PEG and Tween 80 shells. Such disruption facilitates the coalescence of droplets into uncontrolled larger aggregates due to the "over-processing"

effect.[39] These findings robustly reinforce the prevailing principle in nanotechnology that higher energy input does not inherently translate to smaller particle size; rather, successful nano-formulation necessitates a harmonious balance between the rate of droplet breakup and the kinetics of surface stabilization.

2.1.5. Effect of Phase Inversion Temperature (PIT)

Temperature, beyond merely influencing kinetic factors, also serves as a critical thermodynamic control parameter for non-ionic surfactants [40,41]. The comprehensive results presented in Figure 1E, S14, S15 and S16, illustrating the evolution of particle size distribution across varying preparation temperatures, robustly confirm the applicability of the Phase Inversion Temperature (PIT) concept. At 60 °C, the observed particle size was significantly large (146.2 nm) with a high PDI of 0.617, indicating a markedly heterogeneous system. Under these thermal conditions, the polyoxyethylene headgroups of Tween 80 remain extensively hydrated, resulting in a bulky hydrophilic domain that sterically hinders the formation of ultra-small emulsion droplets.[42]

A distinct transition was evident at 70 °C, where the particle size plummeted to 11.0 nm. At this precise thermal threshold, partial dehydration of the Tween 80, chains occurs, fundamentally altering the interfacial film curvature and driving the interfacial tension to a near-zero minimum.[43] This transition facilitates the spontaneous formation of fine droplets without requiring excessive mechanical energy, a phenomenon characteristic of the PIT-driven emulsification process, which ensures both the nanometric scale and the high uniformity of the resulting system.[44]

2.1.6. Evaluation of optimal process and encapsulation efficiency

The rigorously optimized formulation process, comprising a temperature of 70°C, a stirring speed of 900 rpm, and a duration of 30 min, successfully yielded a nano-delivery system characterized by an ultra-small

particle size of approximately 14 nm. Significantly, the Encapsulation Efficiency (EE) for Cordycepin was determined to be 72.4 %, a value substantially higher than the 60.5 % achieved for Adenosine. A detailed structural analysis provides a molecular rationale for this differential encapsulation efficiency. Cordycepin (3'-deoxyadenosine) is distinguished by the absence of a hydroxyl group at the 3' position of the ribose sugar compared to Adenosine. This subtle structural modification renders Cordycepin more hydrophobic and confers greater conformational flexibility.[45] Consequently, Cordycepin exhibits a higher affinity for the hydrophobic micro-domains within the Chitosan-PEG complex core, where it can establish more robust electrostatic interactions and hydrogen bonding. In stark contrast, the higher hydrophilicity of Adenosine leads to its preferential distribution within the hydrated shell layer or at the particle-water interface. This peripheral localization increases the propensity for active compound leakage into the aqueous continuous phase during the self-assembly process. The high-efficiency entrapment of these bioactive nucleosides, despite their differing physicochemical profiles, underscores the versatile "amphiphilic-like" nature of the Chitosan-PEG carrier. This system demonstrates an impressive capacity to protect heat-sensitive and oxidation-prone compounds derived from *Cordyceps militaris*, maintaining their therapeutic integrity within a stable nanostructure.

2.2. Morphology and characterization of the NCCs

Morphology

The determination of the morphology and internal architecture of nanoparticles is paramount for a comprehensive understanding of their stability and functional performance. Figure 2A presents the sized-distribution of NCCs by DLS method with Z-average 14 nm and PDI 0.308. TEM micrographs alongside a proposed structural model of the optimized NCCs. As illustrated in Figure 2B, the nanoparticles exhibit a well-defined spherical morphology with a remarkably uniform size distribution and excellent colloidal dispersion, notably devoid of significant aggregation.

The particle diameters observed via TEM ranged from 11-15 nm, demonstrating exceptional congruence with the DLS data. Such high degree of monodispersity is critical, as it directly governs the system's long-term physical stability and its efficiency in penetrating biological barriers.

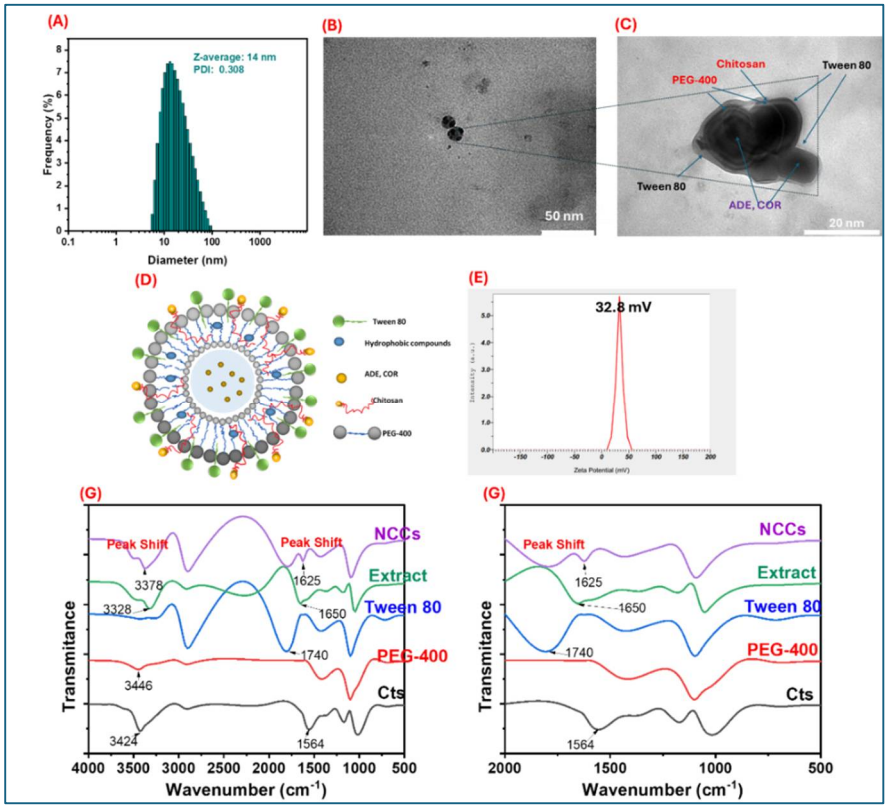

Figure 2. Physicochemical characterization and structural validation of the optimized NCCs formulation. (A) Particle size distribution measured by Dynamic Light Scattering (DLS), showing a Z-average of 14 nm; (B, C) Transmission Electron Microscopy (TEM) micrographs revealing the spherical morphology and internal structure (scale bars: 50 nm and 20 nm, respectively); (D) Proposed structural model of the core-shell NCCs formed via self-assembly; (E) Zeta potential distribution illustrating a positive surface charge of +32.8 mV; (F, G) FT-IR spectra and the corresponding smoothed profiles of NCCs in comparison with individual components (Cts, PEG-400, Tween 80, and *C. militaris* extract), highlighting the characteristic peak shifts as evidence of molecular interactions. *(Formulation parameters: Cts:PEG weight ratio of 7:3, 0.5 % Chitosan, 0.35 % PEG, 3 % Tween 80; homogenized for 30 min at 900 rpm, followed by 1.5 min ultrasonication at 450 W).*

The core-shell structure of NCCs is proved by TEM image (Figure 2C) and hypothesized internal structure (Figure 2D) elucidates a complex

core-shell nano-architecture. The core of these sophisticated particles is theorized to encapsulate the *Cordyceps militaris* extract, which is rich in hydrophilic nucleosides, specifically ADE and COR. The surrounding shell, which effectively partitions the core from the aqueous environment, is formed through the hierarchical self-assembly of Chitosan, PEG-400, and Tween 80. It is posited that PEG-400 and Tween 80 initially facilitate the formation of a primary micellar template via low-energy emulsification. In this phase, the hydrophobic segments of the surfactant and polymer interact with the less polar domains of the extract, while their hydrophilic moieties project outward into the continuous phase.[46] Subsequently, Chitosan owing to its polycationic nature electrostatically anchors onto the negatively charged surface of the pre-formed PEG-Tween 80/extract complex, thereby constructing a robust, positively charged outer integument. This Chitosan layer not only provides electrosteric stabilization but also serves as a protective shield against oxidative degradation while enhancing mucoadhesion to negatively charged cellular membranes.[47] The synergistic integration of PEG and Tween 80 promotes the initial reduction of droplet scale, while the Chitosan shell ensures structural integrity and biological interactivity. This proposed model is in excellent concordance with our experimental observations and aligns with contemporary literature on multi-component polymeric nano-systems.[48]

Furthermore, the surface charge of the optimized NCCs was characterized by a Zeta potential of +32.8 mV (Figure 2E). This strongly positive value provides definitive evidence for the successful architectural assembly of the Chitosan shell. Since PEG and Tween 80 are non-ionic or slightly negative in certain environments, the shift to a high positive

potential is a direct result of the protonated amino groups ($-NH_3^+$) of the Chitosan backbone dominating the particle's external surface.[49]

From a colloidal stability perspective, a Zeta potential around +30 mV indicates a high degree of electrostatic repulsion between individual nanoparticles. This repulsive force effectively counteracts the Van der Waals attractive forces, thereby preventing droplet coalescence and maintaining the long-term physical integrity of the 14 nm system.[50] Moreover, this positive surface charge is strategically advantageous for drug delivery; it facilitates a high affinity for the negatively charged sialic acid residues on mucosal surfaces and cellular membranes, potentially enhancing the cellular uptake and bioavailability of the encapsulated ADE and COR.[51]

FT-IR analysis and molecular interaction validation

To elucidate the molecular interactions driving the self-assembly of NCCs, FT-IR spectroscopy was performed for the nano-system and its individual components. The comparison between the full spectra (Figure 2F) and the partial profiles (Figure 2G) allowed for a precise identification of functional group transformations and peak shifts.

The FT-IR spectrum of raw chitosan (Cts) exhibited a characteristic broad absorption band at 3424 cm^{-1}, corresponding to the overlapping stretching vibrations of hydroxyl (-OH) and primary amine ($-NH_2$) groups.[52] In the NCCs formulation, this band underwent a significant broadening and shifted to a different wavenumber (as indicated by the "Peak Shift" label in Figure 2F), which is a classic indicator of the formation of an extensive intermolecular hydrogen bonding network between the chitosan backbone, PEG-400,[53] and the bioactive molecules from the *C. militaris* extract.

A crucial piece of evidence for the successful encapsulation and molecular rearrangement was observed in the region of 1500 -1700 cm^{-1}.

The *C. militaris* extract showed a prominent peak at 1650 cm^{-1} (attributed to the C=N/C=C stretching of the purine rings in ADE and COR),[54] while raw chitosan displayed a peak at 1564 cm^{-1} (N-H bending vibration of the amine group). Remarkably, in the NCCs spectrum, these two distinct signals converged and shifted to a new peak at 1625 cm^{-1}. This significant peak shift suggests the existence of strong non-covalent interactions, such as electrostatic attractions between the protonated amino groups of chitosan and the electron-rich centers of the nucleosides, as well as potential π-π stacking.[55] Furthermore, the integration of stabilizers into the nano-structure was confirmed by the presence of the ester C=O stretching vibration at 1740 cm^{-1}, originating from Tween 80.[56] Although this peak appeared in the NCCs, its intensity and environment were modified compared to pure Tween 80, suggesting its role in stabilizing the interfacial layer of the nanoparticles. Additionally, the absorption bands in the 1000 - 1100 cm^{-1} region, typical of C-O-C ether linkages from PEG-400 and Tween 80, were clearly visible in the NCCs spectrum, reinforcing the successful formation of the polymeric shell.

The spectral data from Figure 2F and 2G collectively provide robust evidence that the NCCs were not formed through a simple physical blending. Instead, the observed peak shifts and the emergence of hybrid spectral features confirm a self-assembly mechanism facilitated by multi-point non-covalent interactions, effectively "locking" the *C. militaris* bioactives within the chitosan-PEG-Tween 80 framework.

2.3. Evaluation of *NCCs* stability during storage

The long-term storage stability of a nano-delivery system is a pivotal criterion for assessing its practical viability and commercial potential.[57] Figure 3 illustrates the temporal evolution of particle size, PDI, and Zeta

potential of the optimized *C. militaris* nano-system stored under at 4 °C and ambient conditions (25 °C). As illustrated in the Figure 3A, samples stored at 4 °C maintained remarkable structural integrity throughout the 35-day observation period. The average particle size remained nearly constant at approximately 14 - 15 nm, with the PDI fluctuating minimally around 0.31. This stability at lower temperatures can be attributed to the reduction in kinetic energy of the nanoparticles, which effectively inhibits Brownian motion and decreases the frequency of inter-particle collisions, thereby preventing aggregation or Ostwald ripening.

During the initial 30 days of ambient storage, the mean particle size remained remarkably consistent within the range of 14-16 nm, while the PDI exhibited only minor fluctuations between 0.3 and 0.35. This period of kinetic stability demonstrates the system's robust resistance against immediate droplet growth and maintains it monodisperse nature. However, a discernible transition occurred after day 35, where the particle size significantly exceeded 60 nm, accompanied by a rising trend in PDI. This shift marks the onset of destabilization kinetics, signaling the progressive loss of the system's structural integrity.

The electrostatic stability of the NCCs was further evaluated by measuring the Zeta potential at the end of the storage period (day 35). As shown in Figure 3C and 3D, the nanoparticles maintained a positive surface charge, which is a decisive factor for electrosteric stabilization, providing a potent repulsive barrier that prevents particles from approaching within the range of attractive Van der Waals forces.[58] Concurrently, the Zeta potential of samples stored at 4 °C remained highly stable, reinforcing the superior preservative effect of refrigeration on the chitosan-based shell. Even at 25 °C, although the particle size increased due to gradual aggregation, the

residual surface charge continued to provide sufficient steric and electrostatic repulsion to maintain the system's nanoparticulate form. The observed slight decrease in Zeta potential after 35 days at 25 °C correlates directly with the observed aggregation, as the weakened electrostatic repulsion can no longer sufficiently counteract the random thermal collisions (Brownian motion).[59]

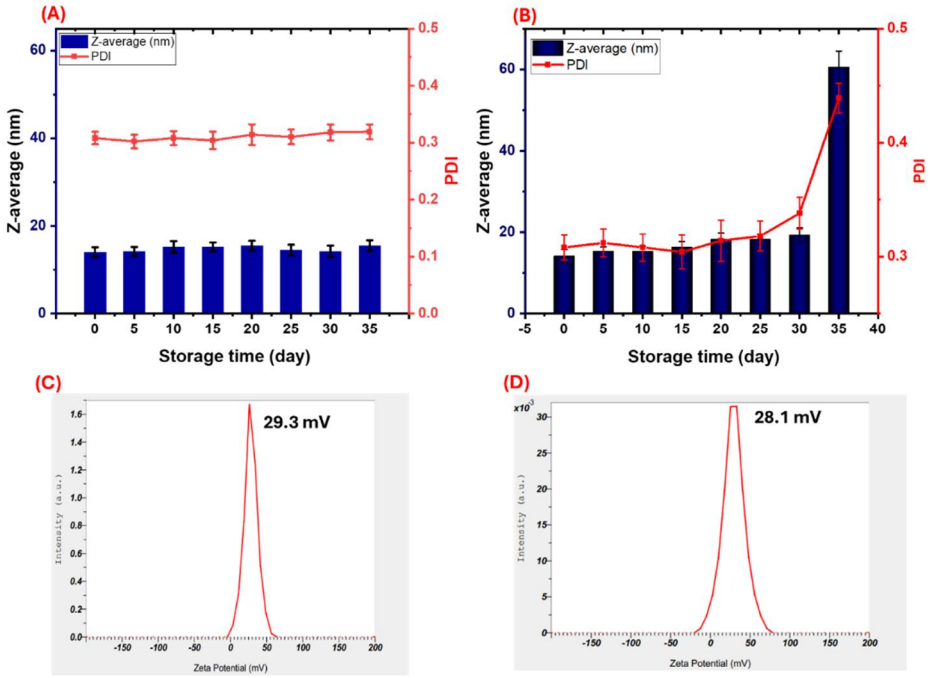

Figure 3. Stability assessment of the optimized NCCs during storage: (A, B) Evolution of Z-average diameter and PDI at 4 °C and 25 °C over 35 days; (C, D) Zeta potential of the NCCs at day 35 under cold-storage (4 °C) and ambient temperature (25 °C), respectively.

The observed instability of the nano-complexes during prolonged storage at ambient temperature can be comprehensively attributed to a synergistic confluence of several physicochemical phenomena. Primary among these is Ostwald ripening, a process fundamentally driven by the Kelvin effect. In this mechanism, smaller droplets, which possess a higher

chemical potential due to their extreme interfacial curvature, gradually dissolve into the continuous phase and subsequently redeposit onto the surface of larger droplets to minimize the system's total interfacial Gibbs free energy [60]. Parallel to this, the system at 25 °C is more susceptible to coalescence and aggregation, triggered by the gradual thinning or displacement of the protective Chitosan-PEG-Tween 80 shell. As the interfacial barrier weakens, the droplets lose their electrosteric protection, allowing them to merge upon collision. Furthermore, the long-term integrity at higher temperatures may be compromised by chemical aging, reducing the interfacial elasticity and mechanical strength of the shell over time.[57]

Despite the onset of instability after 35 days at room temperature, the ability of the NCCs to maintain their physicochemical properties with negligible changes at 4 °C is a highly encouraging result. This demonstrates that refrigeration is a highly effective strategy for extending the shelf-life of these nanocarriers, making them a practically feasible platform for protecting sensitive bioactives from *Cordyceps militaris* in functional food and nutraceutical applications.

2.5. Bioactivity

2.5.1. Antibacterial activity

The antibacterial efficacy of the NCCs was rigorously assessed against two clinically relevant bacterial strains: *Escherichia coli* (Gram-negative) and *Staphylococcus aureus* (Gram-positive), employing the standardized disk diffusion method. Figure 4 illustrates the inhibition zones observed, providing a clear comparative metric of the antimicrobial potency across different formulations. All biological assays were conducted at a uniform concentration of 0.4 % (w/v).

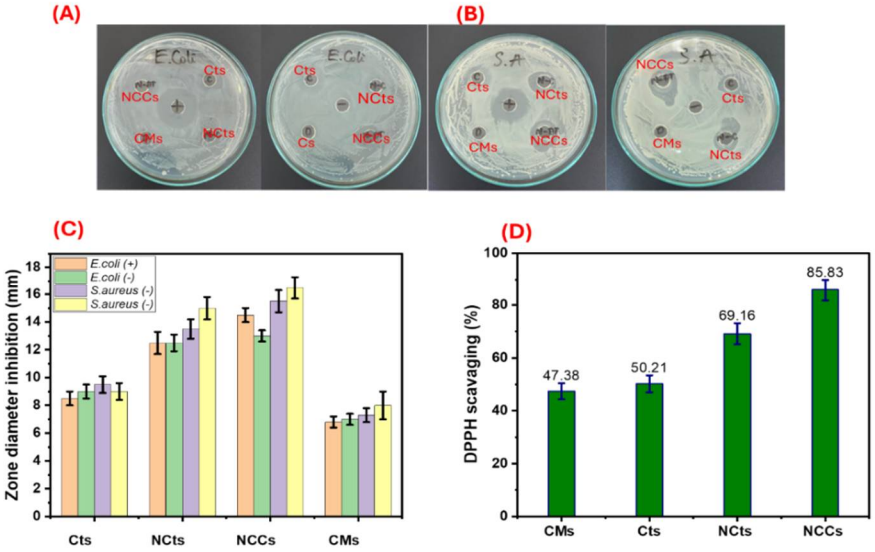

Figure 4. Bioactivity of NCCs and individual components. **(**A), (B) Experimental photographic images illustrating the antibacterial activity against *Escherichia coli* and *Staphylococcus aureus*, respectively; (C) Quantitative measurement of the antibacterial inhibition zone diameters (mm); (D) Free radical scavenging capacity (%).

Upon examination of the experimental data, the diluted *CMs* extract exhibited no discernible zone of inhibition against either strain. This lack of observable activity is likely ascribed to a sub-therapeutic concentration of bioactive metabolites in the diluted state or their rapid degradation within the aqueous experimental environment. Conversely, a progressive increase in antibacterial activity was observed when transitioning from bulk chitosan to its nano-form. Chitosan inherently possesses potent antimicrobial properties primarily due to its polycationic nature. The protonated amine groups ($-NH_3^+$) along the chitosan backbone interact electrostatically with the negatively charged components of bacterial cell membranes (lipopolysaccharides in Gram-negative and teichoic acids in Gram-positive bacteria). This interaction disrupts membrane permeability, leading to the leakage of vital intracellular constituents and subsequent cell death. When

formulated into a nano-architecture, the vastly increased specific surface area and enhanced cellular penetration capacity collectively amplify this inhibitory effect.[61,62]

Most remarkably, the optimized NCCs nano-system consistently demonstrated the most potent antibacterial activity, yielding inhibition zones of 14.5 mm for *E. coli* and a more pronounced 16.5 mm for *S. aureus*. Compared to a previous study by Rupa et al. (2020), which reported inhibition zones of 11 mm and 12 mm respectively,[63] our developed system exhibits superior efficacy, particularly against the Gram-positive strain. This enhancement is robustly attributed to synergistic interactions between the chitosan matrix and the encapsulated bioactive nucleosides COR and ADE from the extract.

Furthermore, the nano-encapsulation plays a pivotal role in shielding these active compounds from environmental degradation while enhancing their solubility and bioavailability in the testing medium. The ultra-small size (~14 nm) facilitates more efficient trans-membrane diffusion, allowing the bioactive cargo to interact directly with internal bacterial targets. The more pronounced effect observed against *S. aureus* compared to *E. coli* is consistent with the structural differences in their cell walls; the absence of an outer membrane in Gram-positive bacteria often renders them more susceptible to the polycationic attack and penetration of chitosan-based nanocarriers.[64] These results unequivocally underscore the potential of the *C. militaris* nano-system as an advanced antimicrobial agent for preservation or therapeutic technologies.

2.5.2. Antioxidant activity

Antioxidant activity is widely recognized as a crucial indicator reflecting the capacity of a bioactive system to neutralize reactive oxygen

species (ROS) and protect cellular components from oxidative stress. Figure 4D provides a comparative analysis of the antioxidant activity, assessed using the DPPH (2,2-diphenyl-1-picrylhydrazyl) method, for the crude *C. militaris* extract, nano-chitosan, and the optimized NCCs nano-system, all evaluated at a uniform concentration of 0.4 % (w/v). The crude *C. militaris* extract exhibited moderate antioxidant activity, consistent with previous research elucidating the radical scavenging capacity of nucleosides like Cordycepin and various polysaccharides present in these fungi.[2] In contrast, the nano-chitosan sample demonstrated significantly higher antioxidant activity compared to the crude extract. Chitosan itself is well-documented for its inherent antioxidant properties, attributable to its polymeric structure containing numerous hydroxyl (-OH) and amine ($-NH_2$) groups, which are capable of scavenging free radicals through hydrogen atom donation.[14,65] When chitosan is formulated into a nano-form, its vastly increased surface-to-volume ratio enhances the accessibility of these functional groups, thereby considerably boosting its radical scavenging efficiency.[66] Most remarkably, the optimized NCCs displayed the highest antioxidant activity among all tested samples, substantially surpassing both the crude extract and the nano-chitosan. The antioxidant capacity of the NCCs was observed to be nearly double that of the crude extract. This superior enhancement is robustly attributed to a confluence of synergistic factors. Firstly, a synergistic effect arises from the combination of antioxidant active compounds (including ADE, COR, and various polyphenols) with the intrinsic antioxidant capacity of the chitosan-PEG carrier.[67] Secondly, the encapsulation within the core-shell nano-architecture effectively shields these sensitive compounds from oxidative degradation induced by environmental factors such as oxygen and light.[68] Thirdly, the ultra-small

nano-size (~14 nm) provides a considerably larger effective surface area for intimate interaction with DPPH radicals. Furthermore, this nanometric dimension facilitates superior penetration and dispersion in the reaction medium, consequently improving the kinetic efficiency of radical scavenging.[58,69]

Conclusion

This study successfully developed and rigorously optimized a complex nano-system specifically designed to encapsulate *Cordyceps militaris* extract, which is notably rich in ADE and COR. The nano-system was meticulously fabricated using a synergistic combination of chitosan, polyethylene glycol (PEG), and Tween 80. This fabrication process involved a systematic, stepwise optimization of critical parameters, including the polymer ratio, surfactant concentration, stirring time, phase inversion temperature, and stirring speed. The culmination of this optimization yielded a nano-system characterized by a remarkably small average particle size of 14 ± 3.7 nm, coupled with an exceptionally low PDI of 0.308, which collectively signifies a highly uniform and stable dispersion. Furthermore, the nano-system demonstrated impressive encapsulation efficiencies, achieving 60.5 % for ADE and a higher 72.4 % for COR, thereby robustly confirming the effective protection and retention of the encapsulated active compounds. TEM imaging further validated the spherical morphology and consistent nano-scale dimensions of the synthesized particles. In terms of stability, the NCCs nano-system maintained stable particle size and PDI for a commendable period of 35 days when stored at room temperature, suggesting its considerable potential for practical applications requiring a reasonable shelf life. Crucially, comprehensive bioactivity assessments unequivocally demonstrated that the NCCs nano-system exhibited

significantly enhanced antioxidant and antibacterial activities when compared to both the crude extract and nano-chitosan alone. This provides compelling evidence for the augmented efficacy of the active compounds when they are effectively encapsulated within this sophisticated nano-structure. These profound findings collectively furnish a robust scientific foundation and unlock promising new avenues for the NCCs nano-system in the progressive development of functional food and pharmaceutical products, offering substantially improved efficacy and bioavailability. Future research endeavors should judiciously focus on evaluating the *in vivo* bioavailability, assessing potential toxicity profiles, and characterizing the controlled release kinetics of this promising nano-system to facilitate its clinical translation.

References

1. Das, S. K.; Masuda, M.; Sakurai, A.; Sakakibara, M. Medicinal uses of the mushroom *Cordyceps militaris*: current state and prospects. *Fitoterapia* **2010**, *81* (8), 961 – 968. https://doi.org/10.1016/j.fitote.2010.07.010
2. Jędrejko, K. J.; Lazur, J.; Muszyńska, B. *Cordyceps militaris*: An overview of its chemical constituents in relation to biological activity. *Foods* **2021**, *10* (11), 2634. https://doi.org/10.3390/foods10112634
3. Tsai, Y. -J.; Lin, L. -C.; Tsai, T. -H. Pharmacokinetics of adenosine and cordycepin, a bioactive constituent of *Cordyceps sinensis* in rat. *J. Agric. Food Chem.* **2010**, *58* (8), 4638 – 4643. https://doi.org/10.1021/jf100269g
4. Zhang, J.; Yang, Z.; Zhao, Z.; Zhang, N. Structural and Pharmacological Insights into Cordycepin for Neoplasms and Metabolic Disorders. *Front. Pharmacol.* **2024**, *15*. https://doi.org/10.3389/fphar.2024.1367820
5. Haskó, G.; Antonioli, L.; Cronstein, B. N. Adenosine metabolism, immunity and joint health. *Biochem. Pharmacol.* **2018**, *151*, 307 – 313. https://doi.org/10.1016/j.bcp.2018.02.002
6. Gutman, D.; Epstein, H.; Koroukhov, N.; Golomb, G. *Liposomal Delivery System of Adenosine for Modulating Inflammation*; 2009; Vol. 19.
7. Lee, J. B.; Radhi, M.; Cipolla, E.; Gandhi, R. D.; Sarmad, S.; Zgair, A.; Kim, T. H.; Feng, W.; Qin, C.; Adrower, C.; Ortori, C. A.; Barrett, D. A.; Kagan, L.;

Fischer, P. M.; de Moor, C. H.; Gershkovich, P. A novel nucleoside rescue metabolic pathway may be responsible for therapeutic effect of orally administered cordycepin. *Sci. Rep.* **2019**, *9* (1), 15760. https://doi.org/10.1038/s41598-019-52254-x

8. Dao, N. Q.; Ba Thanh, N.; Quang Hieu, T. A Study of formulation and characterization of nano liposomes from *Cordyceps militaris* extracts using membrane hydration. *J. Sci. Technol.-IUH* **2025**, *75* (3), 19 – 26. https://doi.org/10.46242/jstiuh.v75i3.5452

9. Nguyen, Q. D.; Tran, K. H.; Nguyen, B. T.; Nguyen, P. T.; Nguyen, M. H.; Tran, Q. H. Novel advanced nanoliposomes incorporating adenosine, cordycepin from Riched-cordyceps militaris extract, and curcumin: formulation, stability, *in vitro* digestion, and enhanced biological activities. *Food Bioprod. Process.* **2025**, *154*, 334 – 349. https://doi.org/10.1016/j.fbp.2025.10.006

10. Akdaşçi, E.; Duman, H.; Eker, F.; Bechelany, M.; Karav, S. Chitosan and its nanoparticles: A multifaceted approach to antibacterial applications. *Nanomaterials* **2025**, *15* (2), 126. https://doi.org/10.3390/nano15020126

11. Kim, H. -M.; Kim, J. -H.; Park, B. -J.; Park, H. -J. Chitosan nanoparticle-encapsulated cordyceps militaris grown on germinated *Rhynchosia nulubilis* reduces type II alveolar epithelial cell apoptosis in $PM_{2.5}$ - Induced lung injury. *Int. J. Mol. Sci.* **2025**, *26* (3), 1105. https://doi.org/10.3390/ijms26031105

12. Moczko, E.; Guerreiro, A.; Piletska, E.; Piletsky, S. PEG - stabilized core – shell surface-imprinted nanoparticles. *Langmuir* **2013**, *29* (31), 9891 – 9896. https://doi.org/10.1021/la401891f

13. Luz, A. M.; Barbosa, G.; Manske, C.; Tavares, F. W. Tween-80 on water/oil interface: Structure and interfacial tension by molecular dynamics simulations. *Langmuir* **2023**, *39* (9), 3255 – 3265. https://doi.org/10.1021/acs.langmuir.2c03001

14. Roy, A.; Mate, C. C.; Kumari, K.; Khatak, D.; Patel, A. K.; Jeza Almotairi, R. M.; Muthupandian, S.; Meena, R. Bovine serum albumin-chitosan nanoparticles loaded with *Cordyceps militaris* extract: A novel approach to combat MDR bacteria. *Microb. Pathog.* **2025**, *205*, 107662. https://doi.org/10.1016/j.micpath.2025.107662

15. Park, B. -J.; Dhong, K. -R.; Park, H. -J. *Cordyceps militaris* grown on germinated *Rhynchosia nulubilis* (GRC) encapsulated in chitosan nanoparticle (GCN) suppresses particulate matter (PM) - induced lung inflammation in mice. *Int. J. Mol. Sci.* **2024**, *25* (19), 10642. https://doi.org/10.3390/ijms251910642

16. Tan, N. T.; Vuong, P. M.; Dao, N. Q.; Dung, T. C.; Nhan, H. T.; Nhu, P. Q.; Dang, N. D. H.; Hieu, T. Q. Novel double nanoemulsion loading of *Cordyceps militaris* extract: formulation, stability, *in vitro* digestion, and *in vivo* evaluation for regulation of acute lipid disorders. *Food Funct.* **2025**, *16* (23), 9080 – 9101. https://doi.org/10.1039/D5FO03188E

17. Dao, N. Q.; Tan, N. T.; Thanh, N. B.; Hung, L. M.; Van My, N.; Hai, N. M.; Tuyen, N. P.; Thang, N. Q.; Dung, T. C.; Hieu, T. Q. Nano-liposome encapsulation of adenosine and cordycepin from *Cordyceps militaris*: preparation, characterization, stability, and *in vitro* digestion evaluation. *Sustainable Food Technology* **2025**, *3* (5), 1341 – 1352. https://doi.org/10.1039/D5FB00146C

18. Thanh, T. N.; Nguyen, Q. D.; Nguyen, D. V.; Nguyen, Q.; Nguyen, M. H.; Nguyen, Q. T.; Phan, M. V.; Pham, Q. N.; Tran, Q. H. Enhanced adenosine and cordycepin extraction from *Cordyceps militaris*: optimization via ultrasound-assisted extraction and response surface methodology. *Acta Chem. Iasi* **2025**, *33* (1), 101. https://doi.org/10.47743/achi-2025-1-0006

19. Tran, Q. H.; Chu, H. K. T.; Nguyen, P. T.; Nguyen, V. M.; Nguyen, Q. T.; Tran, C. D.; Nguyen, T. D. Double nanoemulsion loading betalains extract of beetroot (*Beta vulgaris L.*): ultrasound-assisted synthesis, storage stability, and antioxidant activity. *ACS Food Sci. Technol.* **2023**, *3* (12), 2229 – 2237. https://doi.org/10.1021/acsfoodscitech.3c00430

20. Thang, N. Q.; Hoa, V. T. K.; Van Tan, L.; Tho, N. T. M.; Hieu, T. Q.; Phuong, N. T. K. Extraction of cynarine and chlorogenic acid from Artichoke leaves (*Cynara scolymus L.*) and evaluation of antioxidant activity, antibacterial activity of extract. *Vietnam J. Chem.* **2022**, *60* (5), 571 – 577. https://doi.org/10.1002/vjch.202100117

21. Wu, Y.; Luo, Y.; Wang, Q. Antioxidant and antimicrobial properties of essential oils encapsulated in zein nanoparticles prepared by liquid – liquid dispersion method. *LWT - Food Sci.Technol.* **2012**, *48* (2), 283 – 290. https://doi.org/10.1016/j.lwt.2012.03.027

22. Tran, Q. H.; Doan, T. T. A novel study on curcumin metal complexes: solubility improvement, bioactivity, and trial burn wound treatment in rats. *New J. Chem.* **2020**, *44* (30), 13036 – 13045. https://doi.org/10.1039/d0nj01159b

23. Hieu, T. Q.; Thao, D. T. T. Enhancing the solubility of curcumin metal complexes and investigating some of their biological activities. *J. Chem.* **2019**, 8082195. https://doi.org/10.1155/2019/8082195

24. Hoshyar, N.; Gray, S.; Han, H.; Bao, G. The effect of nanoparticle size on *in vivo* pharmacokinetics and cellular interaction. *Nanomedicine* **2016**, *11* (6), 673 – 692. https://doi.org/10.2217/nnm.16.5

25. Saputra, H. A.; Andreas. Chitosan and its biomedical applications: A review. *Next Mater.* **2025**, *9*, 101270. https://doi.org/10.1016/j.nxmate.2025.101270

26. Fuhrmann, K.; Schulz, J. D.; Gauthier, M. A.; Leroux, J. -C. PEG nanocages as non-sheddable stabilizers for drug nanocrystals. *ACS Nano* **2012**, *6* (2), 1667 – 1676. ACI_389_2025-R2.doc

27. Sahu, A. K.; Mishra, J.; Mishra, A. K. Introducing Tween-curcumin niosomes: preparation, characterization and microenvironment study. *Soft Matter* **2020**, *16* (7), 1779 – 1791. https://doi.org/10.1039/C9SM02416F

28. Quang, T. H.; Tuyen, N. P.; Dao, N. Q.; Quoc Thang, N.; Van Tan, L. Ultrasound-assisted extraction and formulation of Tween 80-curcuminoids nano-micelles for enhanced aqueous solubility and stability. *Acta Chem. Iasi* **2026**, *32* (2), 231 – 258. https://doi.org/10.47743/achi-2025-2-00012%20

29. Lang, C.; Han, B.; Zou, H.; Liu, Z.; Yao, H.; Li, Q.; Chen, H.; Yang, L.; Zhao, J.; Song, Y.; Zhang, L. Characterization of hydrate formation and flow influenced by hydrophilic – hydrophobic components within a fully visual rocking cell. *Energ. Fuels* **2024**, *38* (5), 3670 – 3681. https://doi.org/10.1021/acs.energyfuels.3c04492

30. Karimi, M.; Avci, P.; Ahi, M.; Gazori, T.; Hamblin, M. R.; Naderi-Manesh, H. Evaluation of chitosan-tripolyphosphate nanoparticles as a p-shrna delivery vector: formulation, optimization and cellular uptake Study. *J. Nanopharm. Drug Deliv.* **2013**, *1* (3), 266 – 278. https://doi.org/10.1166/jnd.2013.1027

31. Tsujino, I.; Yamazaki, T.; Masutani, M.; Sawada, U.; Horie, T. Effect of Tween-80 on cell killing by etoposide in human lung adenocarcinoma cells. *Cancer Chemother. Pharmacol.* **1999**, *43* (1), 29 – 34. https://doi.org/10.1007/s002800050859

32. Albashir, M. H.; Mohammed, A. K. Influence of stirring time on the electrochemical synthesis of silver nanoparticles: size and stability analysis. *Int. J. Res. Public. Rev.* **2024**, *5* (5), 10065 – 10070. https://doi.org/10.55248/gengpi.5.0524.1374

33. Thuy, H. T. T.; Ngoc, P. T. K.; Tu, N. T. T.; Truc, H. T. T.; Hai, N. Van; Hieu, T. Q. Comparision of curcumin nanoemulsion drops size between hominization and ultrasonication supporting. *J. Sci. Technol. - IUH* **2020**, *39* (3). https://doi.org/10.46242/jst-iuh.v39i03.277

34. Trofa, M.; D'Avino, G.; Fabiano, B.; Vocciante, M. Nanoparticles synthesis in wet-operating stirred media: investigation on the grinding efficiency. *Materials* **2020**, *13* (19), 4281. https://doi.org/10.3390/ma13194281

35. Walstra, P. Principles of emulsion formation. *Chem. Eng. Sci.* **1993**, *48* (2), 333 – 349. https://doi.org/10.1016/0009-2509(93)80021-H

36. Gupta, A.; Eral, H. B.; Hatton, T. A.; Doyle, P. S. Nanoemulsions: formation, properties and applications. *Soft Matter* **2016**, *12* (11), 2826 – 2841. https://doi.org/10.1039/C5SM02958A

37. Jafari, S. M.; Assadpoor, E.; He, Y.; Bhandari, B. Re-coalescence of emulsion droplets during high-energy emulsification. *Food Hydrocoll.* **2008**, *22* (7), 1191 – 1202. https://doi.org/10.1016/j.foodhyd.2007.09.006

38. Le, X.-T.; Tuan Le, M.; Manh Do, V.; Minh Bui, Q.; Tam Nguyen, A.; Cuong Luu, X.; Nhat Do, D. Fabrication of cajeput essential oil nanoemulsions by phase inversion temperature process. *Mater. Today Proc.* **2022**, *59*, 1178 – 1182. https://doi.org/10.1016/j.matpr.2022.03.190

39. Håkansson, A. Emulsion formation by homogenization: current understanding and future perspectives. *Annu. Rev. Food Sci. Technol.* **2019**, *10* (1), 239 – 258. https://doi.org/10.1146/annurev-food-032818-121501

40. Shinoda, K.; Saito, H. The effect of temperature on the phase equilibria and the types of dispersions of the ternary system composed of water, cyclohexane, and nonionic surfactant. *J. Colloid Interface Sci.* **1968**, *26* (1), 70 – 74. https://doi.org/10.1016/0021-9797(68)90273-7

41. Tran, Q. H.; Thuy, T. T. H.; Nguyen, T. T. T. Fabrication of a narrow size nano curcuminoid emulsion by combining phase inversion temperature and ultrasonication: preparation and bioactivity. *New J. Chem.* **2021**, *45* (21), 9658 – 9667. https://doi.org/10.1039/d1nj01241j

42. Medeiros, M.; Marcos, X.; Velasco-Medina, A. A.; Perez-Casas, S.; Gracia-Fadrique, J. Micellization and adsorption modeling of single and mixed nonionic surfactants. *Colloids Surf. A Physicochem. Eng. Asp.* **2018**, *556*, 81 – 92. https://doi.org/10.1016/j.colsurfa.2018.08.005

43. Anton, N.; Vandamme, T. F. The Universality of low-energy nano-emulsification. *Int. J. Pharm.* **2009**, *377* (1–2), 142 – 147. https://doi.org/10.1016/j.ijpharm.2009.05.014

44. Izquierdo, P.; Esquena, J.; Tadros, Th. F.; Dederen, C.; Garcia, M. J.; Azemar, N.; Solans, C. Formation and stability of nano-emulsions prepared using the phase inversion temperature method. *Langmuir* **2002**, *18* (1), 26 – 30. https://doi.org/10.1021/la010808c

45. Jaiswal, J.; Srivastav, A. K.; Rajput, P. K.; Yadav, U. C. S.; Kumar, U. Integrating Synthesis, Physicochemical Characterization, and In Silico Studies

of Cordycepin-Loaded Bovine Serum Albumin Nanoparticles. *J. Agric. Food Chem.* **2023**, *71* (32), 12225 – 12236. https://doi.org/10.1021/acs.jafc.3c03608

46. Jiang, J.; Wang, Z.; Wang, C.; Shi, L.; Hou, J.; Zhang, L. Effect of nonionic surfactants on the synergistic interaction between asphaltene and resin: Emulsion phase inversion and stability. *Colloids Surf. A Physicochem. Eng. Asp.* **2023**, *675*, 132056. https://doi.org/10.1016/j.colsurfa.2023.132056

47. Klinkesorn, U. The role of chitosan in emulsion formation and stabilization. *Food Rev. Int.* **2013**, *29* (4), 371 – 393. https://doi.org/10.1080/87559129.2013.818013

48. Al-Zuhairy, S. A. S.; Teaima, M. H.; Shoman, N. A.; Elasaly, M.; El-Nabarawi, M. A.; El-Sawy, H. S. PEGylated Tween 80-functionalized chitosan-lipidic nano-vesicular hybrids for heightening nose-to-brain delivery and bioavailability of metoclopramide. *Drug Deliv.* **2023**, *30* (1). https://doi.org/10.1080/10717544.2023.2189112

49. Shariatinia, Z. Pharmaceutical applications of chitosan. *Adv. Colloid Interface Sci.* **2019**, *263*, 131 – 194. https://doi.org/10.1016/j.cis.2018.11.008

50. Ofir, E.; Oren, Y.; Adin, A. Electroflocculation: the effect of zeta-potential on particle size. *Desalination* **2007**, *204* (1 – 3), 33 – 38. https://doi.org/10.1016/j.desal.2006.03.533

51. Bhattacharjee, S. DLS and zeta potential – What they are and what they are not? *J. Control. Release* **2016**, *235*, 337 – 351. https://doi.org/10.1016/j.jconrel.2016.06.017

52. Chen, G.; Mi, J.; Wu, X.; Luo, C.; Li, J.; Tang, Y.; Li, J. Structural Features and Bioactivities of the Chitosan. *Int. J. Biol. Macromol.* **2011**, *49* (4), 543 – 547. https://doi.org/10.1016/j.ijbiomac.2011.06.009.

53. Smith, R. A.; Walker, R. C.; Levit, S. L.; Tang, C. Single-step self-assembly and physical crosslinking of PEGylated chitosan nanoparticles by tannic acid. *Polymers (Basel).* **2019**, *11* (5), 749. https://doi.org/10.3390/polym11050749

54. Roy, A.; Mate, C. C.; Kumari, K.; Khatak, D.; Patel, A. K.; Jeza Almotairi, R. M.; Muthupandian, S.; Meena, R. Bovine serum albumin-chitosan nanoparticles loaded with *Cordyceps militaris* extract: A novel approach to combat MDR bacteria. *Microb. Pathog.* **2025**, *205*, 107662. https://doi.org/10.1016/j.micpath.2025.107662

55. Wen, Y.; Li, Y.; Liu, T.; Sun, C.; Zhao, H.; Yuan, Y.; Yang, S.; Zhao, T.; Liu, J. Nucleoside-based hydrogel platform synergizes with photothermal effects for enhanced biofilm eradication against periodontitis. *Adv. Sci.* **2026**, *13* (13). https://doi.org/10.1002/advs.202522853

56. Haghani, I.; Raeisabadi, A.; Akhtari, J.; Arbabi, A.; Abastabar, M.; Hedayati, M. T.; Yahyazadeh, Z.; Talebpour Amiri, F.; Hashemi, S. M. H.; Davoodi, L.;

Nezhad, Y. H.; Siahposht-Khachaki, A.; Bandegani, A.; Rahimnia, S. M.; Badali, H. Innovative green niosomal piperlongumine as a novel topical treatment for dermatophytosis in guinea pigs model. *Sci. Rep.* **2025**, *15* (1), 37829. https://doi.org/10.1038/s41598-025-21729-5

57. Hou, J.; Huang, T.; Alotaibi, M.; AlSofi, A. Long-term thermal stability of ionic surfactants for improving oil production at high-salinity high-temperature conditions. *ACS Omega* **2024**, *9* (10), 11976 – 11986. https://doi.org/10.1021/acsomega.3c09734

58. McClements, D. J. Advances in edible nanoemulsions: Digestion, bioavailability, and potential toxicity. *Prog. Lipid Res.* **2021**, *81*, 101081. https://doi.org/10.1016/j.plipres.2020.101081

59. Russel, W. B. Brownian motion of small particles suspended in liquids. *Annu. Rev. Fluid Mech.* **1981**, *13* (1), 425 – 455. https://doi.org/10.1146/annurev.fl.13.010181.002233

60. Khedr, A.; Striolo, A. Quantification of ostwald ripening in emulsions via coarse-grained simulations. *J. Chem. Theory Comput.* **2019**, *15* (9), 5058 – 5068. https://doi.org/10.1021/acs.jctc.9b00296

61. Raafat, D.; Sahl, H. Chitosan and its antimicrobial potential – a critical literature survey. *Microb. Biotechnol.* **2009**, *2* (2), 186 – 201. https://doi.org/10.1111/j.1751-7915.2008.00080.x

62. Qi, L.; Xu, Z.; Jiang, X.; Hu, C.; Zou, X. Preparation and Antibacterial Activity of Chitosan Nanoparticles. *Carbohydr. Res.* **2004**, *339* (16), 2693 – 2700. https://doi.org/10.1016/j.carres.2004.09.007

63. Rupa, E.; Li, J.; Arif, M.; Yaxi, H.; Puja, A.; Chan, A.; Hoang, V.-A.; Kaliraj, L.; Yang, D.; Kang, S. *Cordyceps militaris* fungus extracts-mediated nanoemulsion for improvement antioxidant, antimicrobial, and anti-inflammatory activities. *Molecules* **2020**, *25* (23), 5733. https://doi.org/10.3390/molecules25235733

64. Sotelo-Boyás, M. E.; Correa-Pacheco, Z. N.; Bautista-Baños, S.; Corona-Rangel, M. L. Physicochemical characterization of chitosan nanoparticles and nanocapsules incorporated with lime essential oil and their antibacterial activity against food-borne pathogens. *LWT* **2017**, *77*, 15 – 20. https://doi.org/10.1016/j.lwt.2016.11.022

65. Xie, W.; Xu, P.; Liu, Q. Antioxidant Activity of Water-Soluble Chitosan Derivatives. *Bioorg. Med. Chem. Lett.* **2001**, *11* (13), 1699 – 1701. https://doi.org/10.1016/S0960-894X(01)00285-2

66. Divya, K.; Smitha, V.; Jisha, M. S. Antifungal, antioxidant and cytotoxic activities of chitosan nanoparticles and its use as an edible coating on vegetables. *Int. J. Biol. Macromol.* **2018**, *114*, 572 – 577. https://doi.org/10.1016/j.ijbiomac.2018.03.130

67. Vashitha, A.; Khan, S. S. Recent advances in the development of chitosan based nanocarriers for drug delivery application: Critical challenges, outlooks and promises in cancer therapy. *Int. J. Biol. Macromol.* **2025**, *321*, 146184. https://doi.org/10.1016/j.ijbiomac.2025.146184

68. Shamloo, E.; Sadeghi, E.; Soltani, M.; Mahmoudifar, K.; Taghizadeh, M.; Arab, M.; Abdi-Moghadam, Z.; Rezagholizade-Shirvan, A.; Shokri, S. Encapsulation of natural/bio-based materials as nano bio-adsorbents for removal of toxic pollutants from food products: A review. *Carbohydr. Polym. Technol. Appl.* **2025**, *10*, 100870. https://doi.org/10.1016/j.carpta.2025.100870

69. Tran, Q. H.; Le Thi, T. T.; Nguyen, T. C.; Tran, T. V.; Le, Q. T.; Luu, T. T.; Dinh, V. P. Facile synthesis of novel nanocurcuminoids – sacha inchi oil using the phase inversion temperature method: Characterization and antioxidant activity. *J. Food Process. Preserv.* **2021**, *45* (5). https://doi.org/10.1111/jfpp.15402